Supplementary Materials:

S1. Stereophotoclinometry and Digital Elevation Determinations.
     The image sets used for examining area A and B are taken from narrow angle camera (NAC) images acquired by the Lunar Reconnaissance Orbiter Camera (LROC). Stereophotoclinometry (SPC) is a technique developed by Robert Gaskell to generate a Digital Elevation Model (DEM). SPC combines the benefits of stereo positioning and photoclinometry to generate image pixel to DEM pixel resolutions. The uncertainty of the height or vertical position is the same as the horizontal resolution of the DEM. A low resolution DEM was generated for area A at 2.5 m/px and area B at 2.6 m/px, and covered an area about 9 x 9 km. Higher resolution strips of 0.8 m/px cover an area 3.75 x 9 km for area A, and of 0.7 m/px that cover an area 0.9 km x 9 km for area B. The NAC is a linescan imager, and acquires images in strips with a large aspect ratio, with the long axis oriented along the spacecraft trajectory, typically in a North-South orientation on LRO. As such, the high resolution DEM strips were also oriented North-South. This way the entire DEM could be generated from a single image set. Otherwise, the Eastern portion would be generated from the coverage of one image set and the Western portion from the coverage of another image set. Using a single image set slightly increases the fidelity of the DEM because a small error could be introduced during the transition between the two image sets.

Table S1 - **LROC NAC Images of Ingenii Swirl Study Areas**	
Images used in Area A	Images used in Area B
M1102510544L*	M1097788036R
M1102510544R*	M105802305L*
M1124891128L*	M105802305R
M1124891128R*	M112883561L*
M164791607R	M112883561R
M115252292L*	M1120165013L*
M115252292R*	M1120165013R
M1109583890L	M1128423456L*
M1109583890R	M1128423456R
M1124884018R*	M1133137598R
M1135504503L	M1137843545L

M1097795227L*	M1137843545R*
M184825229R	M1137850655L
M180107476L	M1137850655R*
M180107476R*	M1163750779L*
M1137857807R*	M1163750779R
M184818082R	M1163757893R
	M1168464712R*
	M1183744016L*
	M1183744016R
	M1183758218L*
	M189528774L
	M1220258422L*
	M1220258422R
	M1220265455L*
	M1220265455R
	M1220272488L*
	M1220272488R
	M1222607556L
	M1224963678L
	M1235522307L
	M1235522307R*
	M1235529339L
	M1235529339R*

	M1242583258L*
	M1242583258R
	M1270799282R
	M1281411275R*
* Indicates images used in high resolution DEM	

A description of the basics of SPC follows. The fundamental unit of SPC is called a maplet, which is a 99 x 99 pixel representation of the topography, with the value of each maplet pixel giving the height of the surface. The center pixel of the maplet is defined from the images by stereo positioning. Essentially, a pixel is found in each image that corresponds to the same patch of ground. A ray is then extended from each pixel, and where the rays cluster defines the center pixel position of the maplet. This position minimizes the error in distance to each ray, with higher resolution images weighted more heavily.

The remaining maplet pixels are defined from the images via photoclinometry. The brightness of each image pixel is determined by the albedo of the surface and the slope of the surface. Bright pixels in the image could be due to high albedo, or the surface tilting towards the spacecraft camera. Dim pixels in the image could be due to low albedo, or the surface tilting away from the camera. High incidence images emphasize the albedo of the surface, while low incidence images emphasize the topography of the surface. Photoclinometry uses images with different incidence angles to solve for both the albedo and slope for each maplet pixel. The height of the center maplet pixel and the slope of each maplet pixel is then integrated to determine the height for all remaining maplet pixels.

In essence, stereophotoclinometry combines the highly accurate absolute position of a stereo solution, with the high-resolution relative position of a photoclinometric solution. In rare situations, usually with poor images sets, photoclinometry will have larger height errors during transitions between areas of low and high albedo. However, these larger errors would only occur between two stereo positions, and will not have a significant affect on the overall heights of on- and off-swirl regions.

Tens of thousands of maplets were used to cover the high resolution strips presented here. Each maplet has a portion of topography that overlaps with adjacent maplets, and the heights of overlapping maplets are used to ensure the photoclinometric uncertainty remains small at the edges. These overlaps are important since any errors in the slope will compound the uncertainty as the height solution progresses outward from the stereo-defined center pixel.

After the maplets are generated, the next important process in SPC is to update the spacecraft position when an image was acquired. Once the position and height of many maplets has been determined, we essentially perform the reverse of the stereo solution. Instead of using multiple images to define the center position of a maplet, we use many maplets to define the position of the spacecraft for each image. This updated spacecraft

position can then be used to further refine the stereo position of each maplet, which in turn can be used to refine the spacecraft position. Thus, SPC becomes an iterative solution between the topography and the spacecraft position. During all of these iterative processes, the alignment of images within each maplet is continually refined.

Once the topography and spacecraft positions no longer improve with successive iterations, the maplets are combined into a single DEM for distribution.

S2. Mapping and Processing of DEM datasets.

DEM data products in equidistant cylindrical projection and GeoTiff file format were imported into ESRI ArcGIS Desktop 10.4 software (ArcGIS) for the following tasks: 1) mapping of on- and off-swirl regions, 2) regional slope corrections, 3) crater and feature masking, 4) output of topographic data for statistical analyses, and 5) creation of high-resolution DEM strips for both study areas. ArcGIS is a commercial Geographic Information Systems package with a large and robust set of tools for image processing, mapping, 3-D viewing and geostatistical analysis of both raster and vector-based geographic data.

Mapping of On and Off-Swirl Regions
Using the LROC WAC basemap in ArcGIS, the on-swirl regions for study areas A and B were manually digitized based on tonal differences between the bright swirl and surrounding darker terrain. Because the tonal difference is often subtle at the transition from bright to dark, the mapped boundary should be considered approximate. In study area A, the off-swirl sub-region is much larger than the on-swirl. In order to make roughly comparable regions in terms of number of data points, we created two separate off-swirl sub-regions (off-swirl1 and off-swirl2) that are concentric to the on-swirl region. Off-swirl1 extends 750 m beyond the on-swirl margin and off-swirl2 extends 850 m beyond the off-swirl1 margin. For study area B, the mapped on-swirl region is much larger than off-swirl. Thus, creating off-swirl sub-regions was not necessary.

Regional Slope Correction in Topographic Data
Regional slopes of less than 0.5 degree are apparent from NW-SE profiles across the full DEMs for study areas A and B. For study area A, the slope trends up from NW to SE, particularly for the last third of the profile ending at the SE corner (Fig. S1). For study area B, the slope trends down for the entire length of the NW-SE profile (Fig. S1). In order to remove potential slope bias, we corrected for the regional slope in each study area with the following steps below.

Using a Global Polynomial Interpolation method within the ArcGIS Geostatistical Analyst extension package, a raster "subtraction" surface was created. This method creates a best-fit surface to the input topographic data based on a first-order polynomial. It is analogous to a best linear fit to the surface that captures the coarse-scale pattern (i.e. slope) in the dataset, but without the localized topographic features such as impact craters, hills, pits, etc. While higher-ordered surfaces can be generated to follow natural bends in the surface topography, a simple first-order polynomial was sufficient for the two study areas. The subtraction surfaces were generated on early lower resolution DEMs for areas A (5 m and 2.5 m) and B (2.6 m), but then re-scaled to the higher resolution topography (80 cm and 70 cm, respectively for areas A and B) for slope subtraction in those datasets.

Because the topography generated at the different resolutions are derived from the same core stereophotoclinometry results, there is no change to the inherent slope, regardless of resolution.

To assess the fit of the first-order interpolated surface to topography, a standard least-squares linear regression model was applied to the output data. For study area A with a total of 3,316,041 elevation points, the predicted versus actual values produces a correlation coefficient (a.k.a., r-squared value) of 0.700 with a mean of -4.137×10^{-7} m and a standard error of 10.4 (Fig. S2). For study area B with a total of 11,992,369 elevation points, the predicted versus actual values produces a correlation coefficient of 0.915 with a mean of -1.196×10^{-8} m and a standard error of 12.3 (Fig. S2). In slope intercept form, the model is:

$$y^2 = 0.700x - 1057 \ (study \ area \ A)$$

$$y^2 = 0.915x - 293 \ (study \ area \ B)$$

The high coefficient for study area B indicates that the majority of data points in the subtraction surface are a good fit to the original topographic data and provides confidence that the synthetic surface closely matches the observed slope. The lower coefficient for study area A is expected since only one-third of the profile showed a slope with the remaining parts relatively flat.

Subtraction surface values at the SE corner of each study area were compared to the original topographic values within a 3x3 pixel area so that the surface could be adjusted to match the original as closely as possible, creating a "zero" base level prior to slope subtraction. For study area A, 30 meters were added to the synthetic surface and for study area B, 4 meters were added. After adjusting the surface, the slope was subtracted from the original topographic data; thus, producing final slope-corrected elevations (Fig. S3).

Crater and Feature Masking
Impact craters create localized extreme data values in both the topography and albedo, which have a negative cumulative effect on the statistical analyses. To mask out such values, we first identified all craters down to 50 m diameter in the WAC basemap and albedo map, including any as part of a crater chain. Using circular or elliptical selection tools in ArcGIS, the full area of each crater, including the approximate crater rim, was traced and saved as a polygon shapefile. Then, using the raster "clip" function in ArcGIS, the areas of all mapped craters were masked out for the slope-corrected topography (Fig. S4). In addition to craters, large geologic features up to several hundreds of meters across, such as pits and hills (unrelated to masked craters), were also mapped and masked out (see Fig. S4). Craters smaller than 50 m diameter were not masked since they represent a small fraction of the total surface area and do not have depths that would significantly affect our analysis.

Individual pixel values from the slope-corrected, crater-masked topographic data were exported to space-delimited ASCII text files for statistical analysis. The pixel values for on- and off-swirl regions were exported separately for both study areas.

High-Resolution DEM strips

In addition to the lower resolution datasets that fully cover study areas A and B, higher resolution DEM tiles were produced for a portion of each study area. For study area A, 80 cm/pixel DEM tiles were imported into ArcGIS in a 2x5 column arrangement (see text Figure 1). For study area B, 70 cm/pixel tiles were imported as a 1x10 column (see text Figure 2). All tiles were available as GeoTiff format files in an equidistant cylindrical projection, each with its own defined central meridian and standard parallel.

In study area A, the pixel values were spot checked along a two-to-three pixel overlap between DEM tiles along their northern edge. Values were generally within an acceptable 1-20 cm difference in elevation. Holding the northernmost tile as fixed, each subsequent tile was manually shifted to align pixels in the overlapping region between tiles. After this adjustment, tiles in each column were placed in order from north to south to produce a single DEM strip. Because the tiles are in an equidistant cylindrical map projection, the horizontal distance of each pixel fractionally increases the further south from the northernmost tile. Thus, along both the western and eastern edges of the column, up to three pixels with zero values were added to account for the horizontal distance. These pixels were then changed to no-data values to prevent errors in the statistical analyses. After production of the two DEM strips, the overlap region between the two were manually shifted to align pixels (eastern edge of column one, western edge of column two). Due to the map projection, the overlap at any given spot ranges between one to five pixels. The elevation difference between pixels was generally less than 5 cm.

In study area B, the pixel values were spot checked along a one pixel overlap between DEM tiles and were generally within an acceptable 1-10 cm difference in elevation. As in the case with study area A, each tile below the northernmost tile was then manually shifted to match pixels in the overlapping region. The remaining steps followed the same process, save for the last due to only a single DEM strip for this area.

We note that the same slope correction, crater and feature masking, and on- and off-swirl data export steps as described above was applied to each high-resolution DEM strip for statistical analysis.

S3. Statistical Analysis Methodology and Application.

For the high-resolution topographic data, in study area A at 80-cm, the pixel counts were 7714871 for on-swirl and 9756854 for off-swirl1 and off-swirl2. In study area B at 70-cm, the pixel counts were 8092842 for on-swirl and 3671097 for off-swirl.

The non-parametric Kolmogorov-Smirnov (K-S) test is a measure of the difference between two cumulative distributions. We use Kuiper's variant, which increases the sensitivity of the test in the tails of the probability distribution. Kuiper's statistic, V, is the sum of the maximum distances of one dataset, $S_{N1}(x)$, above and below the second dataset, $S_{N2}(x)$:

$$V = \max_{-\infty < x < \infty} |S_{N1}(x) - S_{N2}(x)| + \max_{-\infty < x < \infty} |S_{N2}(x) - S_{N1}(x)|$$

where x is height and N_1 and N_2 are the number of points in each dataset. The significance of the results is based on the null hypothesis that the datasets come from the same parent and is given by the K-S statistic, $V\sqrt{N}$, where $N=N_1 N_2/(N_1+N_2)$. We empirically calibrated

the K-S statistic by comparing a hundred thousand randomly selected samples of the size of our smallest dataset to a uniform distribution: 1-, 2-, and 3-sigma levels correspond to cumulative probabilities of 84.1%, 97.7%, and 99.9% at $V\sqrt{N}$ values of approximately 1.5, 2 and 2.5, respectively.

For the K-S test on the cumulative distributions of topography in study area A, the on-swirl versus off-swirl1 yields $V\sqrt{N}$ =378 and versus off-swirl2 yields $V\sqrt{N}$ =597. For the cumulative distributions in study area B, the on-swirl versus off-swirl yields $V\sqrt{N}$ =620. These results represent a confidence level of greater than four sigma that the on- and off-swirl topographic datasets are not drawn from the same samples at either study area A or B.

Our datasets are each samples pulled from larger populations of data. To quantify the difference in the mean heights of the datasets, we derive a confidence interval assuming independent samples with unknown but equal population variances. The resulting value with error bars is the range in which the population mean difference is expected to be, to a given percentage accuracy. Our samples sizes are large, therefore we use the Z score, based on the cumulative standard normal distribution, for the selected confidence interval. The mean difference in heights between datasets h_1 and h_2 is given by

$$\left(\overline{h_1} - \overline{h_2}\right) \pm z_{\alpha/2} \sqrt{\frac{\sigma_p^2}{N_1} + \frac{\sigma_p^2}{N_2}}$$

where $z_{\alpha/2}$ is the reliability factor, 1-α is the percentage confidence interval, and σ_p is a pooled estimate of the combination of the standard deviations of the two datasets (σ_{h1} and σ_{h2}):

$$\sigma_p = \sqrt{\frac{(N_1 - 1)\sigma_{h1}^2 + (N_2 - 1)\sigma_{h2}^2}{N_1 + N_2 - 1}}$$

For 95% confidence intervals, in study area A, the mean of the on-swirl heights is 2.386±0.005 m lower than off-swirl1 and 4.475±0.005 lower than off-swirl2. In study area B, the mean of the on-swirl heights is lower than off-swirl by 2.640±0.004 m. Note that the results are identical if we do not use the pooled estimate and instead assume the standard deviations of the samples reflect the variance of the populations.

As an additional investigation, we created histograms of the topographic data and fit the binned data with Gaussians defined as

$$a\ exp\left(-\frac{(h - \mu)^2}{2\sigma^2}\right)$$

where a is a constant, h is the height, μ is the mean, and σ is the standard deviation. Note that we do not assume that the topography follows a normal distribution, but the function is used here because it is a good approximation to the shapes of the histograms. The best-fit values for each dataset are provided in Table 2.
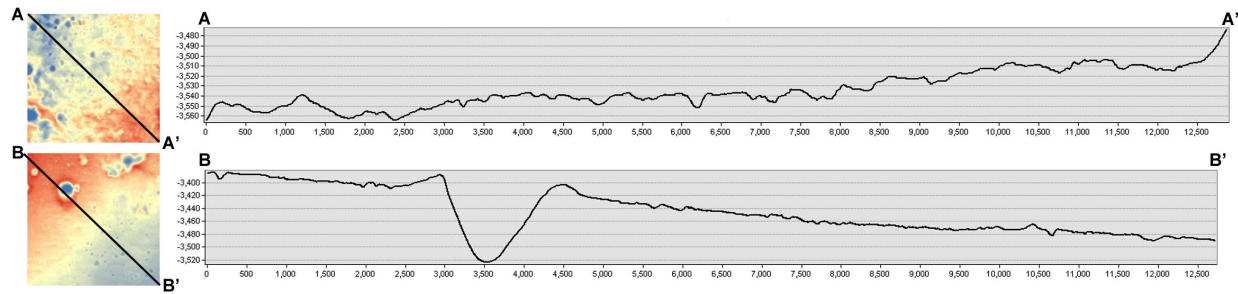
Figure S1. NW-SE topographic profiles across Ingenii study areas A and B with regional slopes of less than 0.5⁰. For study area A (top), the profile (A-A') has a slope trending up in the latter one-third of the profile ending at the SE corner. The profile (B-B') for study area B (bottom) slopes down over the entire distance of the profile. Topographic data with lower elevations are in blue and higher elevations are in red. North is up. Elevations and distances for each profile are in meters.
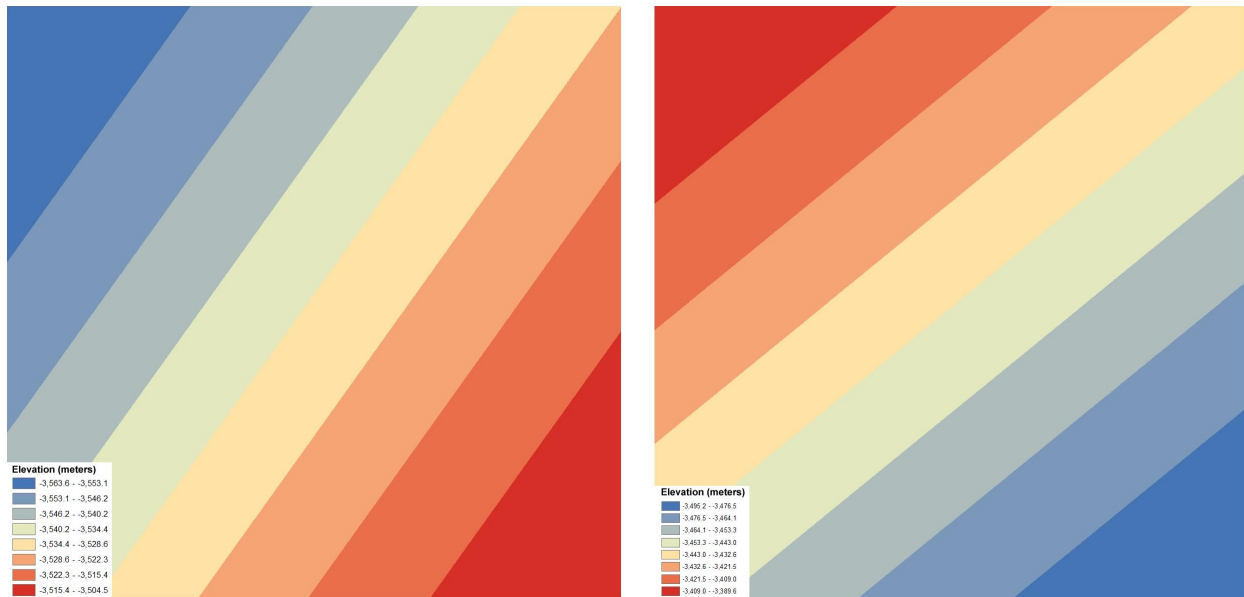

Figure S2. Raster subtraction surfaces generated using a first-order global polynomial interpolation method applied to the original ~2.5 m/pixel DEMs for Ingenii study areas A (left) and B (right). The trend direction follows the NW-SE regional slope observed in the topographic profiles (see Fig. S1). North is up in both panels.
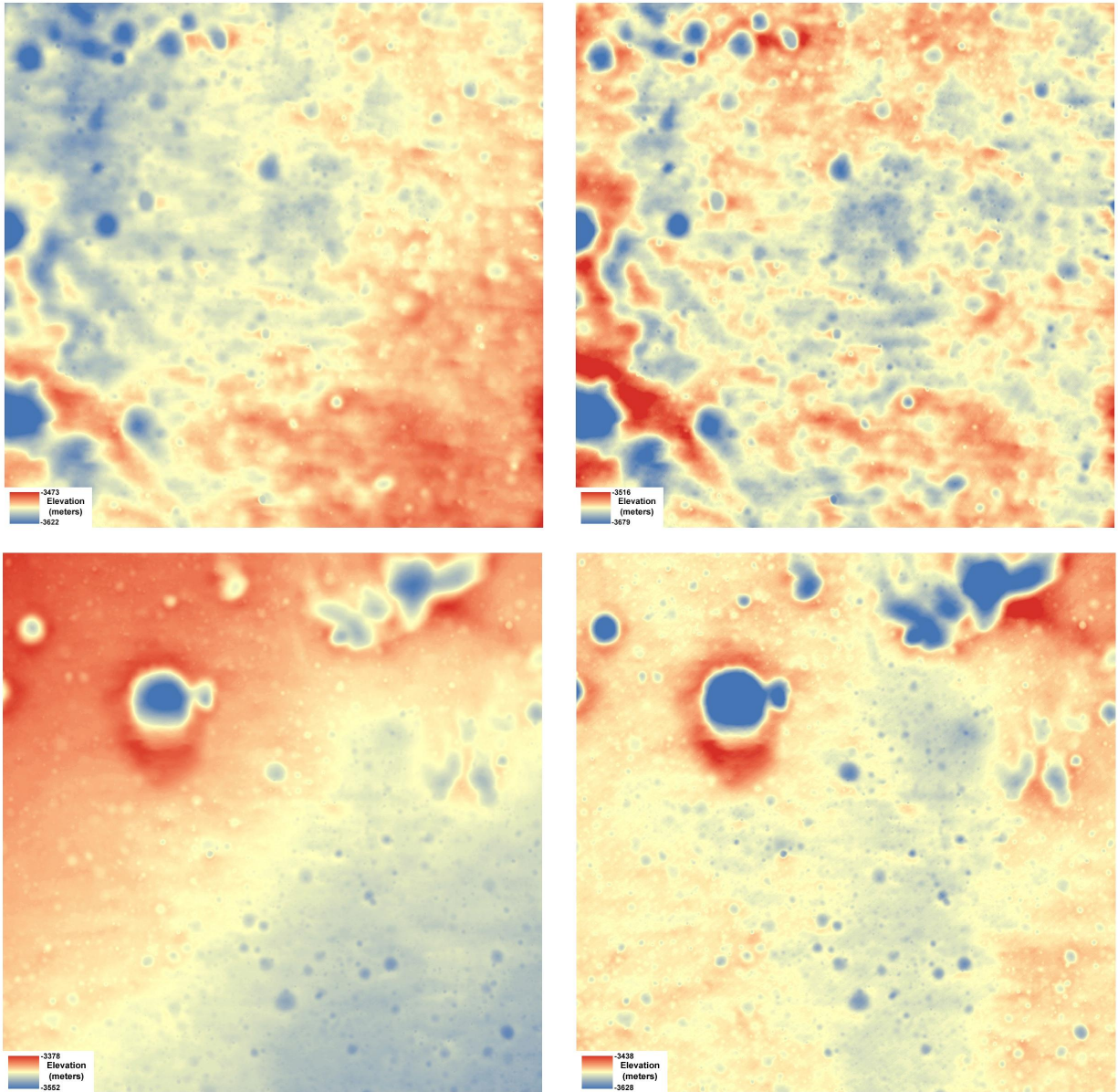
Figure S3. Original (left) and slope-corrected (right) topography for Ingenii study areas A (top panels) and B (bottom panels). Colorized topography in all panels have an applied linear stretch over 3 standard deviations of the mean. Width of each panel is ~9 km and north is up.
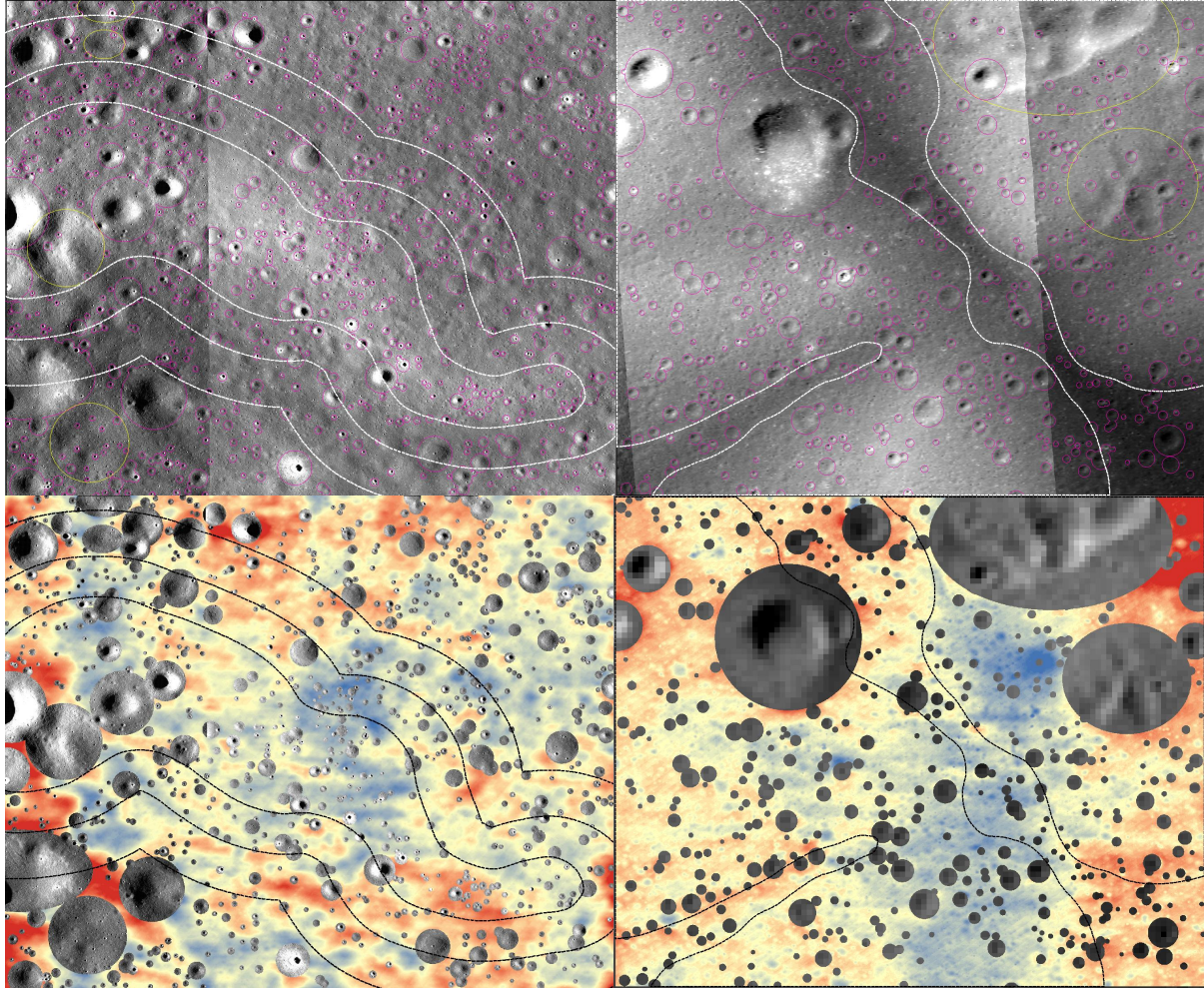
Figure S4. (Top) Albedo maps of study areas A (left) and B (right) with mapped impact craters down to ~50 m diameter (magenta) and larger non-crater features (yellow) identified from both albedo and topography data. **(Bottom)** Slope-corrected ~2.5 m/pixel topography data of study areas A (left) and B (right) with impact craters and non-crater features masked out. Colorized topography in both panels have an applied linear stretch over 3 standard deviations of the mean. Width of each panel is ~9 km and north is up.

Table S2.

Region	Constant (a)	Mean (μ; m)	Standard deviation (σ)	Full-width at half maximum (m)
Swirl Area A				
on-swirl	$4.33(\pm0.22)\times10^5$	-3565.09 ± 0.34	5.85 ± 0.34	13.78 ± 0.34
off-swirl1	$7.30(\pm0.25)\times10^5$	-3562.40 ± 0.19	4.66 ± 0.19	10.97 ± 0.19
off-swirl2	$5.28(\pm0.08)\times10^5$	-3561.41 ± 0.10	5.91 ± 0.10	13.93 ± 0.10
Swirl Area B				
on-swirl	$7.12(\pm0.07)\times10^5$	-3493.33 ± 0.03	2.43 ± 0.03	5.71 ± 0.03
off-swirl	$2.71(\pm0.12)\times10^5$	-3490.66 ± 0.18	3.60 ± 0.18	8.47 ± 0.18